The Effects of Nonlinear Jetting in Super Resolution Focusing of Sound Among a Helmholtz Resonator Array

Mark Carlisle

A senior thesis submitted to the faculty of
Brigham Young University
In partial fulfillment of the requirements for the degree of

Bachelor of Science

Brian E. Anderson, Advisor

Department of Physics and Astronomy

Brigham Young University

ABSTRACT

The Effects of Nonlinear Jetting in Super Resolution Focusing
of Sound Among a Helmholtz Resonator Array

Mark Carlisle
Department of Physics and Astronomy,
BYU Bachelor of Science

Time reversal (TR) is a technique used to focus wave energy to a selected location. High energy TR focusing has application in biomedical ultrasound and nondestructive evaluation of cracks or defects in solids. These applications can benefit from having the narrowest possible spatial extent of the focused sound energy, which is normally diffraction limited. Two-dimensional Helmholtz resonator arrays placed in the near field of TR focusing have been shown to produce a sub-diffraction limited spatial extent of the focused energy (when compared to the free-space wavelength). There is an apparent amplitude dependence to this focusing and this thesis will discuss these nonlinear aspects. These observations were made by analyzing experimental results of TR focusing among an array of empty soda cans at different sound excitation levels. These nonlinear effects occur at much lower sound levels than is typical for nonlinear waveform steepening. The conclusion is made that the nonlinear observations are acoustic nonlinearities and are likely caused by acoustic jetting in Helmholtz resonators and this principally causes the amplitude of the focusing to be as much as three times lower in amplitude than linear scaling would predict and causes the spatial extent of the focusing to increase.

Keywords: time reversal, resonator array, non-linear, diffraction limit

ACKNOWLEDGEMENTS

I would like to thank Brian E Anderson for mentoring me over the past year and a half, Bryce Lundstrom for helping with the experimental setups, The College of Computational, Mathematical, and Physical sciences for funding me and making this research possible. I'd like to thank my wife for supporting me and encouraging me through all of this.

Contents

List of Figures

Chapter 1

Introduction

Time reversal (TR) is a technique used in acoustic signal processing to focus wave energy to a desired location.[1-4] TR is akin to beamforming in that multiple sources can be timed or phased delayed to achieve high amplitude focusing of waves, but with TR the timing of the loudspeaker emissions is achieved by reversing an initial recording, thereby avoiding the need to calculate delays for each loudspeaker used. In the TR process there is a forward step and a backward step when creating TR focusing. In the forward step, an impulse response is obtained, one at a time, between source transducers and a receiver. In the backward step, each source transducer outputs its respective reversed impulse response signal, obtained in the forward step. TR exploits multiple scattering (many reflections) to its advantage because of the time reversal operation and thus utilizes all these reflections as if there were additional image sources in addition to the real loudspeaker sources. The result is a constructive interference of many waves at the target or focusing location. The spatial extent of the focus is diffraction limited with a half wavelength

diameter being the smallest width possible; however, due to the so-called point spread function inherent in the waves collapsing to a single point, the spatial extent is typically closer to a wavelength in diameter.

High energy focusing[5] is one of the primary uses of TR and has application in biomedical ultrasound,[6-8] non-destructive evaluation of cracks or defects in solids,[4,9] and some demonstrations include knocking over a targeted LEGO minifigure[10,11] and blowing out a targeted candle.[12] TR can also be used for source imaging applications to locate gun shots in urban environments[13,14] and to locate and characterize earthquakes.[15-18] Communication of signals to a target is another application of TR and has application to active control of noise[19] and private communication.[20-22] It is important in these applications to minimize the spatial extent of the focused sound energy to achieve better resolution when delivering high amplitude energy, imaging a complex source, and delivering a targeted signal to a precise location.

The spatial extent of TR focusing is characterized by the size of the wavelength. The higher the frequency used in TR, the smaller the wavelength and thus the tighter the focus can be; however, increasing the frequency is not the only way to tighten the focus. Resonator arrays placed in the near field of TR focusing have been shown to produce a sub-diffraction limited spatial extent of the focused energy (when compared to the free-space wavelength). An electromagnetic wave experiment had an arrangement of resonating copper wires which resulted in a $\lambda/30$ spatial resolution.[23] Using soda cans, Lemoult *et al.*[24] was able to achieve a $\lambda/8$ spatial resolution with acoustic waves and after introducing iterative TR methods was able to achieve $\lambda/25$. Lemoult *et al.*[25] then showed that the soda can array can be considered a phononic crystal and can control wave propagation in unique ways. They further showed that several modes among the array of cans superpose to create this sub-diffraction limited focusing. Maznev *et al.*[26] showed that time

reversal wasn't technically needed to achieve focusing if the loudspeakers were equidistant from the focusing location. Lemoult *et al.*[27] then described the band gap properties that the soda can array can have and described the array as a metamaterial. Maznev and Wright[28] then argued that the diffraction limit is not broken in experiments like these but rather the fundamental wave speed among a resonator array is decreased and thus the diffraction limit isn't technically being broken. In the present study, we recognize that the resonator array changes the effective wave speed, but we adopt the typical convention of comparing the spatial extent of the focusing among a resonator array to the free-space wavelength and term this sub-diffraction limited or super resolution focusing, even if technically the diffraction limit is not being broken. Orazbayev and Fleury[29] used a resonator array to communicate numbers with subwavelength resolution.

Recent research at Brigham Young University has included Kinsley *et al.*[30] exploring various shapes of resonators, using electrical equivalent circuit modeling, to optimize their shape for optimal TR focusing and found that the soda can possesses fortuitous dimensions for achieving high quality subwavelength focusing. Kingsley and Anderson[31] then showed agreement with their circuit modeling and full-wave, finite-element modeling and showed visually how each resonator slows down waves that propagate among the resonators. Kingsley *et al.*[32] then showed experimentally how complex sources could be constructed, with subwavelength precision, when focused near an array of soda cans. Finally, Basham *et al.*[33] showed that the spatial extent of the focusing could be reduced even further when using a two-dimensional waveguide or wavefield decomposition analysis. In this later study, they asserted that it's the waves that travel in the plane of the array that principally contribute to the reduction of the spatial extent. The waveguide restricted the incident waves to be in the plane of the array and wavefield decomposition could alternatively be used in post processing (without using a waveguide).

Previous research has shown that TR focusing at higher amplitudes results in localized nonlinear wave activity at the focal location. Sometimes this has resulted in a change in the frequency spectrum (i.e. harmonics or sum and difference frequencies) as well as a nonlinear change in amplitude. An extensive summary of the use of these nonlinear effects for nondestructive evaluation can be found in Ref. 4. Nonlinear features were shown in TR focusing by Montaldo *et al.*[34] though they did not study them further. Nonlinear characteristics have been observed in focusing of audible sound waves at levels upwards of 170 dB and can cause nonlinear amplification of compressions and nonlinear suppression of rarefactions due to the formation of Mach stems.[35-37] These high amplitude waves in air have been used to generate a difference frequency[38] and extinguish flames.[12]

Though nonlinear characteristics are normally seen at high sound levels, there is a phenomenon known as jetting that can occur in Helmholtz resonators at much lower sound levels than the levels required to observe Mach stem formation or nonlinear waveform steepening. Jetting is a term used to describe a phenomenon that occurs with higher amplitude excitation of Helmholtz resonators. Russell[39] provided various visual demonstrations of jetting occurring at sound levels of just 121 dB. Helmholtz resonators produce a net stream of air directed away from the neck opening along the axis of the neck. This occurs because the movement of the mass in the neck outward generally pushes the air along the axis of the neck while the movement of air inward will pull air from all directions. Over the course of a cycle of the resonance frequency, the time-averaged, net result is a force outward from the neck of the resonator. The authors believe that this jetting causes nonlinear phenomena in TR focusing among a soda can array at sound levels as low as 100 dB.

The purpose of this thesis is to describe the nonlinear effects that this jetting phenomenon has when focusing among a Helmholtz resonator array; meaning that several properties of the

focusing are amplitude dependent. This nonlinearity chiefly results in lower amplitudes at the focus point than would be expected from linear scaling. The spatial extent of the focus also increases slightly at higher amplitudes. The jetting is confirmed visually by observing the motion of candle flames placed near a soda can in the array and then blowing out the candle in the direction directly away from the can opening when a sufficiently high amplitude focus of sound is created.

Chapter 2

Methods

All tests carried out for the experiments described in this work were done in Brigham Young University's large reverberation chamber. The dimensions of the chamber are 4.96 x 5.89 x 6.98 m with a reverberation time of 6.85 s for the bandwidth of frequencies used. The reverberation chamber has a Schroeder frequency of approximately 355 Hz. Above this, the chamber is assumed to have a diffuse field. The Helmholtz resonator array is made up of 127 soda cans in a hexagonal arrangement. These cans have magnets epoxied to their bottom to allow any custom arrangement on a steel plate that is held vertically in the setup. The magnets are strongly attracted to the steel plate to prevent sliding but not too strong so that they can be rearranged as desired. The steel plate is placed on a 1.82 m by 0.91 m board of wood that stands up vertically. Eight HR824mk2 Mackie (Seattle, WA) loudspeakers are randomly placed 0.91 m above the floor and spaced equally around the walls of the chamber and are pointed towards the wall to minimize the dominance of the direct sound in the reversed impulse response.[40] The microphones used are

a 12.7 mm (1/2 inch) GRAS (Holte, Denmark) random-incidence and a 6.35 mm (1/4 inch) GRAS free-field microphone. A computer-controlled gantry is used to position a microphone at discrete locations across the array, enabling scans of the sound field. The microphone is mounted at the end of a metal pole attached to the gantry scanning system as shown in Figure 2.1.

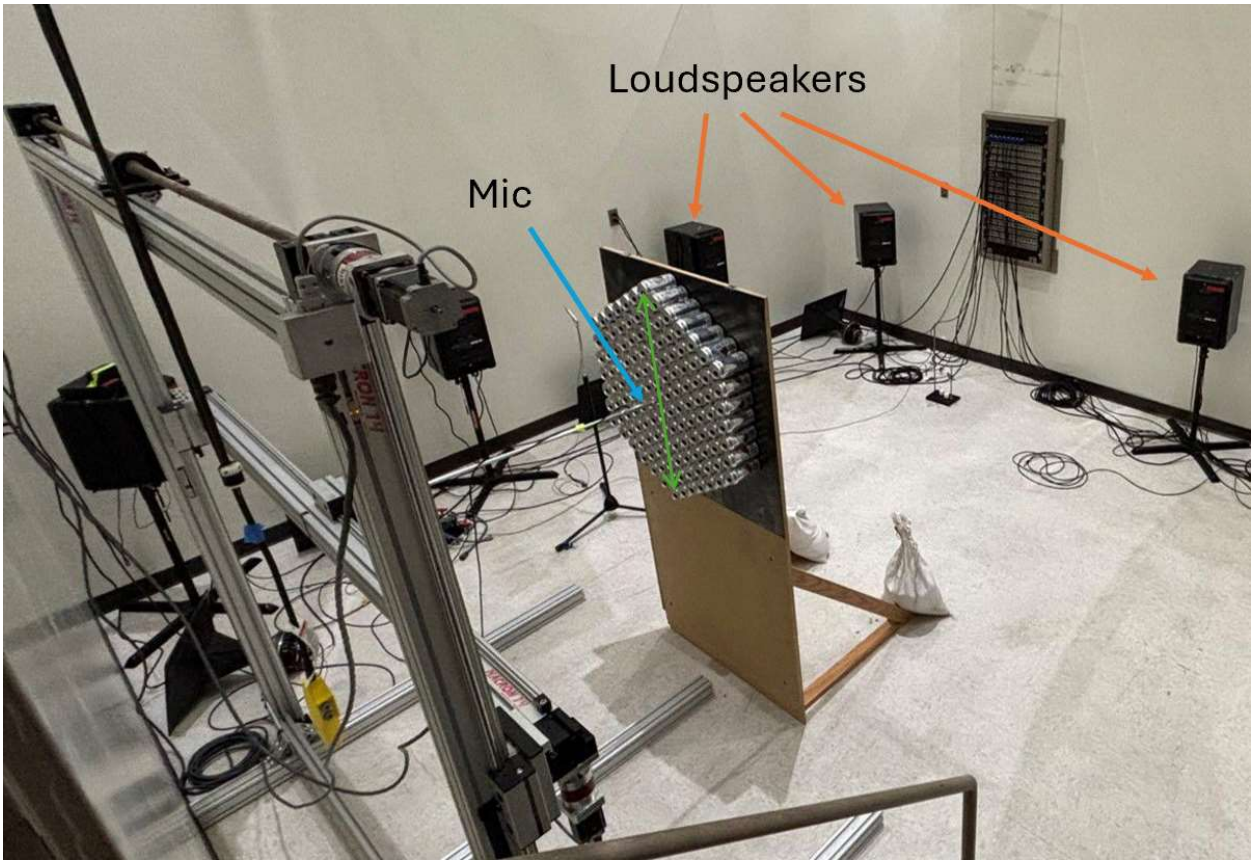

Figure 2.1 Photograph of the setup used to measure nonlinear characteristics when using time reversal to focus among a resonator array. It involves 8 loudspeakers, a scanning system, a 127 soda can resonator array, and a microphone, all in a reverberation chamber.

Typical signals used in the steps of TR focusing are shown in Figure 2.2. A chirp signal, ranging from 350 Hz to 420 Hz is first broadcast by a loudspeaker (see Figure 2.2(a)). 350 Hz was chosen since it is near the Schroeder frequency in the room, and 420 Hz was chosen since it is

approximately the Helmholtz resonance frequency of an individual empty soda can. Subwavelength focusing has been shown to occur for frequencies below the Helmholtz resonance frequency of a single resonator. The response to this chirp signal broadcast is recorded by the microphone (an example is shown in Figure 2.2(b)). An impulse response can then be calculated between this loudspeaker and the microphone using a cross-correlation operation.[40,41] If multiple loudspeaker sources are used, the impulse responses are obtained one at a time. Reversed impulse responses (an example is shown in Figure 2.2(c)) are then broadcast simultaneously from the respective loudspeakers. TR focusing is then produced at the microphone location, appearing as the impulsive spike in amplitude (see an example in Figure 2.2(d)). Custom, in-house software, called ESTR developed within LabVIEW (Austin, TX), is used to broadcast and record these signals as it was designed for TR experiments.[42] Time averaging was used when recording TR focusing, to enhance the signal-to-noise ratio (10 averages were used).

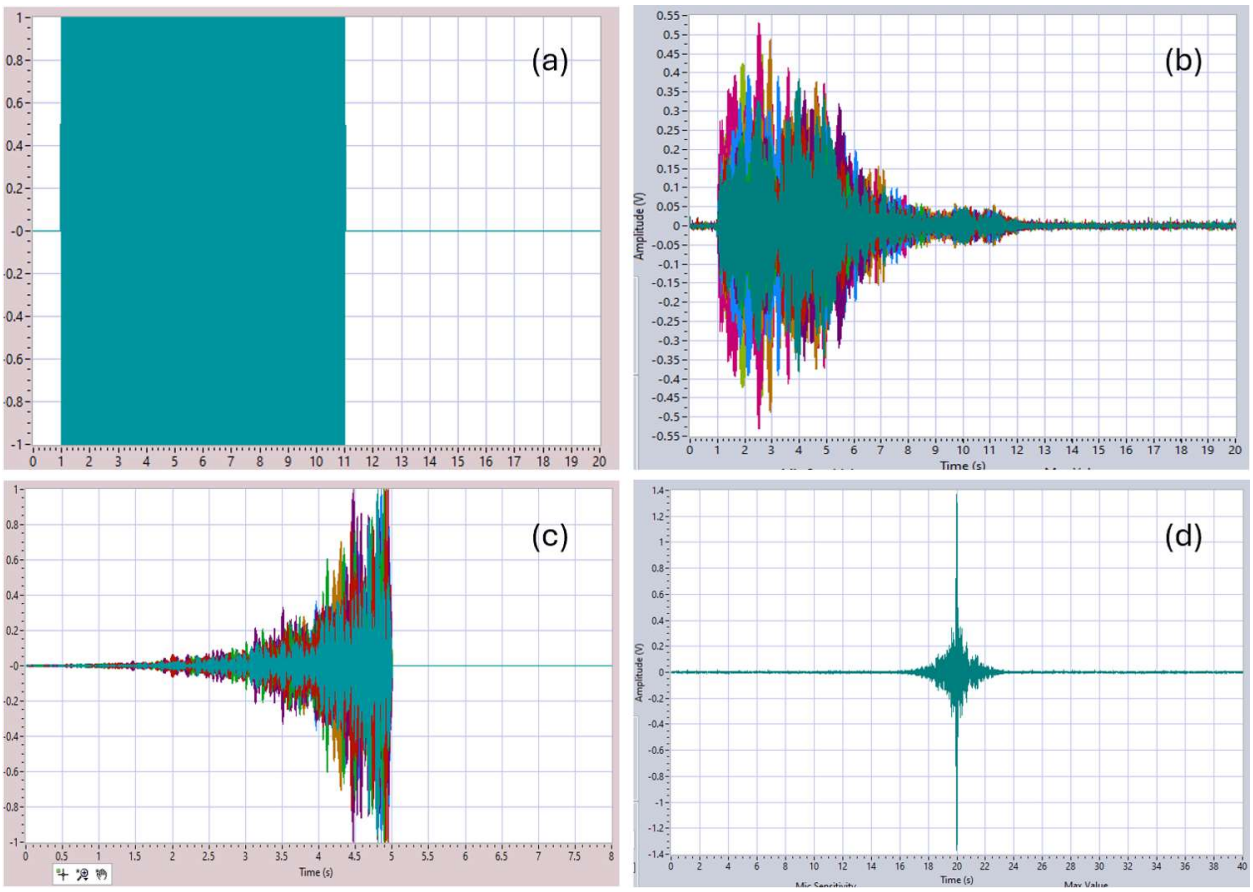

Figure 2.2 Time reversal forward (parts (a) and (b)) and backward (parts (c) and (d)) steps. (a) Shows the initial impulse signal. (b) Recorded impulse responses from each speaker overlayed on the same graph. (c) The impulse response reversed in time. (d) The recorded focus.

The authors wished to ensure that the presence of the microphone near a can opening did not significantly alter the sound field by constricting the opening (potentially even extending the effective length of the acoustic mass in the neck) and skew the recording of the TR focusing results. To optimize the microphone placement, a microphone was placed right at the mouth of the central can and slowly backed away, along the axis of the can, up to 5 cm away in 5 mm increments (see Figures 2.3(a) and 2.3(b)). A full new TR experiment was done at each microphone position. The authors took great care to ensure that the microphones were placed at the same locations for each scan. The recordings of focusing made by the two different sized

microphones were compared by subtracting the recordings (that should be identical if the microphone is not disturbing the sound field), squaring the subtraction result, and then summing the squared values to determine a total squared error between the two microphone signals. This total squared error is plotted in Figure 2.3(c). A microphone standoff distance of 2 cm was chosen as the optimal distance where the difference in output of the 6.35 mm and 12.7 mm microphones was deemed small enough to not significantly perturb the sound field, but still close enough to the array to obtain the sub-diffraction limit TR focusing.

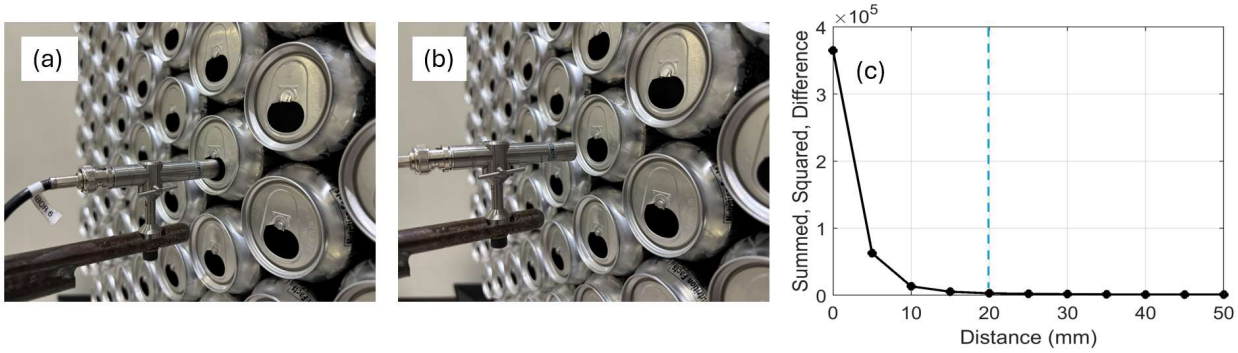

Figure 2.3 Experimental setup for optimal microphone distance. Photographs of the microphone placed (a) at 0 cm from the opening and (b) at 2 cm from the opening are shown and a graph (c) showing the total squared difference in outputs of the two microphones as they were pulled away from the array. The blue dashed line marks where the microphones were deemed to agree sufficiently.

Chapter 3

Results

The results presented in this chapter describe how the nonlinearities found in this study are acoustic nonlinearities and how they affect the amplitude of the focusing and overall spatial extent of the focused sound energy. Evidence of jetting is also shown.

Amplitude differences in TR focusing as a function of input amplitude to the loudspeakers were tested by focusing to a point in space far away from the resonator array and redoing the TR focusing very near the resonator array (new forward and backward steps were conducted for each setup). Once the impulse responses were obtained, the input amplitudes to the loudspeakers playing these signals were increased starting at 100 mV and increasing up to 1000 mV in 100 mV increments and the TR focusing was recorded. Graphs of acoustic pressure versus time are given in Figure 3.1 with the pressure amplitudes unscaled and linearly scaled to compare differences in amplitude. In Figure 3.1(a) we see that the higher the input voltage to the loudspeakers, the higher the amplitude of the focusing when the microphone is far away from the Helmholtz resonator array.

In Figure 3.1(b) we see the same focusing results, though this time they are linearly scaled, and it is apparently that the focusing signals do in fact scale linearly, as expected. Then the resonator array is placed such that the center can is 2 cm from the microphone and a new set of TR experiments are done with varying input amplitudes for the focusing. In Figure 3.1(c) we observe that the focusing amplitude again increases with increasing input voltage amplitude and we can observe that the peaks seem to steadily arrive earlier in time with increasing input voltage. In Figure 3.1(d) these data are linearly scaled and this time our scaled results do not linearly scale as they did in (b). The peak amplitude in the focus signal when using 1 V input amplitude is 3 times lower than the linearly scaled peak amplitude in the focus signal when using 100 mV input amplitude. This nonlinear suppression trend is steadily observed for all input amplitudes, that as we increase the input amplitude, we get less focusing amplitude than expected for linear scaling and the compressions and rarefactions both arrive earlier in time, demonstrating that this certainly is not a linear system when the cans are near the TR focusing. However, linear scaling is observed when the cans are not present near the TR focusing, demonstrating that the source of the nonlinearity is acoustic. The amplitudes when the cans are not present are actually larger than when the cans are present, so the nonlinearity cannot be the result of mechanical or electrical distortions, since one would expect larger mechanical or electrical nonlinearities with higher amplitude, no matter what state the acoustic environment is in. Rattling noise from the cans, which was not observed, would exist at higher frequencies than 420 Hz and would not be as perfectly repeatable as these nonlinear features are. When considering the amplitudes shown in Figure 3.1, it may be helpful to know that a root-mean-square pressure amplitude of 50 Pa corresponds to a sound pressure level of 128 dB, which is approximately the level of the highest amplitude focusing when

the cans are not present and the amplitude of the focusing for 100 mV input amplitude reaches approximately a sound level of 110 dB.

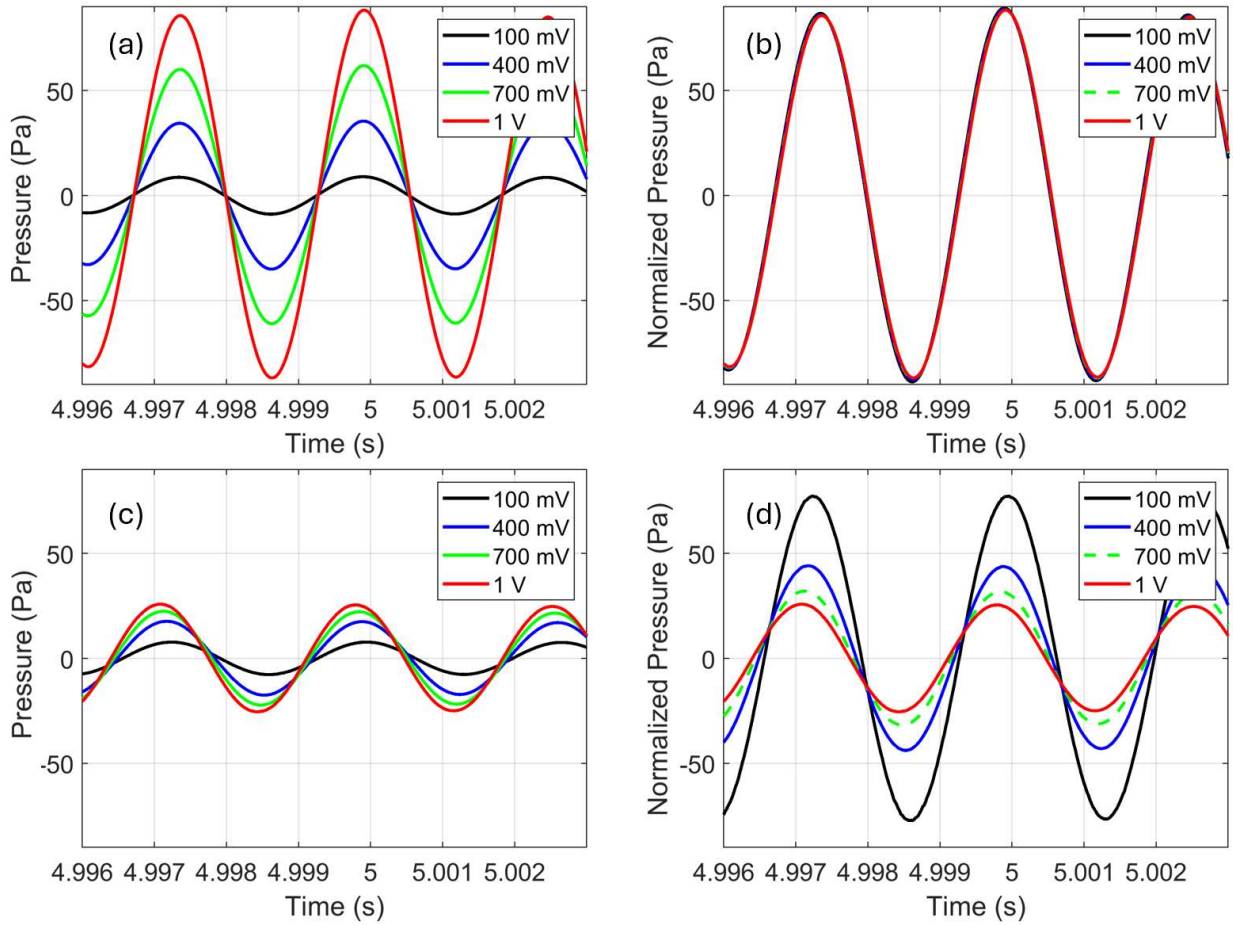

Figure 3.1 Graphs of recorded pressure amplitudes when focusing sound with different input voltages. Duplicate data is graphed that has been linearly scaled to 1 V for comparison when focusing away from the array ((a) and (b)) and to the array ((c) and (d)).

A simple experiment was used to test for jetting. A candle was lit and placed at the TR focusing location when the cans were present. Cliftmann and Anderson[12] showed that levels of at least 170 dB were required in this same reverberation chamber to blow out a candle placed at the location of TR focusing. With our 1 V input amplitudes to the loudspeakers, which produces a sound level of 122.2 dB, the flame is visibly pushed away from the cans in a steady fashion. During

TR focusing, the flame is oscillating small amounts but it is also noticeable leaning to the side for about 30 ms during the highest amplitude of the focusing, as would be expected with jetting (see Figure 3.2). If the mass in the neck of the resonator was moving without jetting, the candle would not have a net outward displacement (compare Figures 3.3(a) and 3.3(b)).

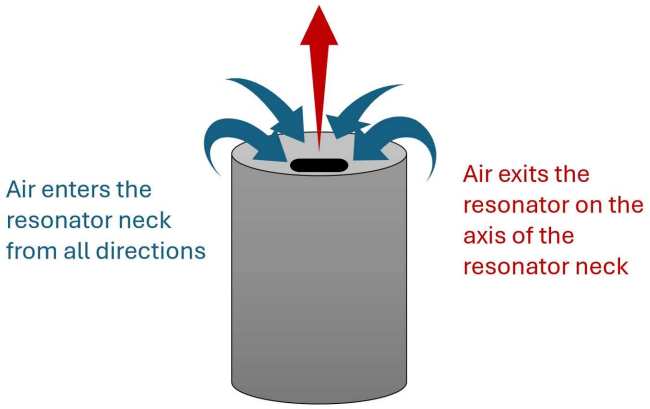

Figure 3.2 Arrows show external air flow directions at the neck of a Helmholtz resonator during resonance at high amplitudes. The air is drawn into the neck from all directions and expelled primarily in the direction of the neck's axis as a jet of air.

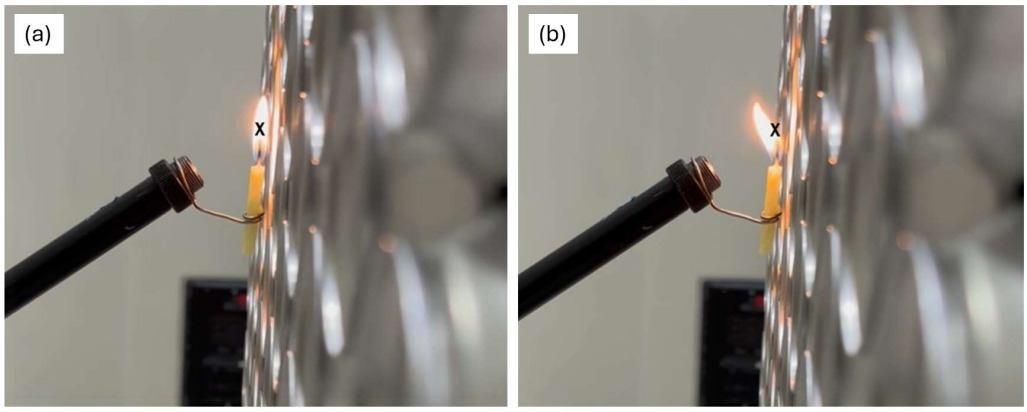

Figure 3.3 Photographs of a candle lit next to the Helmholtz resonator array. (a) the candle is stationary until the sound is focused, then in (b) the flame is pushed outward (throughout the focusing event, whether compressions or rarefactions are occurring at this location), away from the array, demonstrating the jetting effect. The x shows the point of focus.

We then added the clipping TR method[10,35] to increase the TR focusing amplitude without increasing input voltage. Now the TR focusing reaches an amplitude of approximately 140 dB and the flame was extinguished, as seen in Figure 3.4 (with a different lighting in these images than in Figure 3.3). Part (a) shows the normal flame before focusing and part (b) shows the flame being pushed outward. Then in parts (c) and (d) we can observe that the flame has been blown out and the smoke trail being is pushed noticeably to the left, which is visible in these images (note that the brightness and contrast of parts (c) and (d) has been altered to better visualize the smoke). These visual observations further supports that jetting is occurring during TR focusing when the resonator array is present. If the resonator array were not present, the candle flame barely moves at all, as studied extensively by Cliftmann and Anderson.[12] This result of the candle flame being extinguished at a level of just 140 dB is also significant since Cliftmann and Anderson found that blowing out a candle flame without a resonator array present required a minimum of 170 dB, though the flame was not repeatably blown out unless the TR focusing amplitudes reached more than 180 dB.

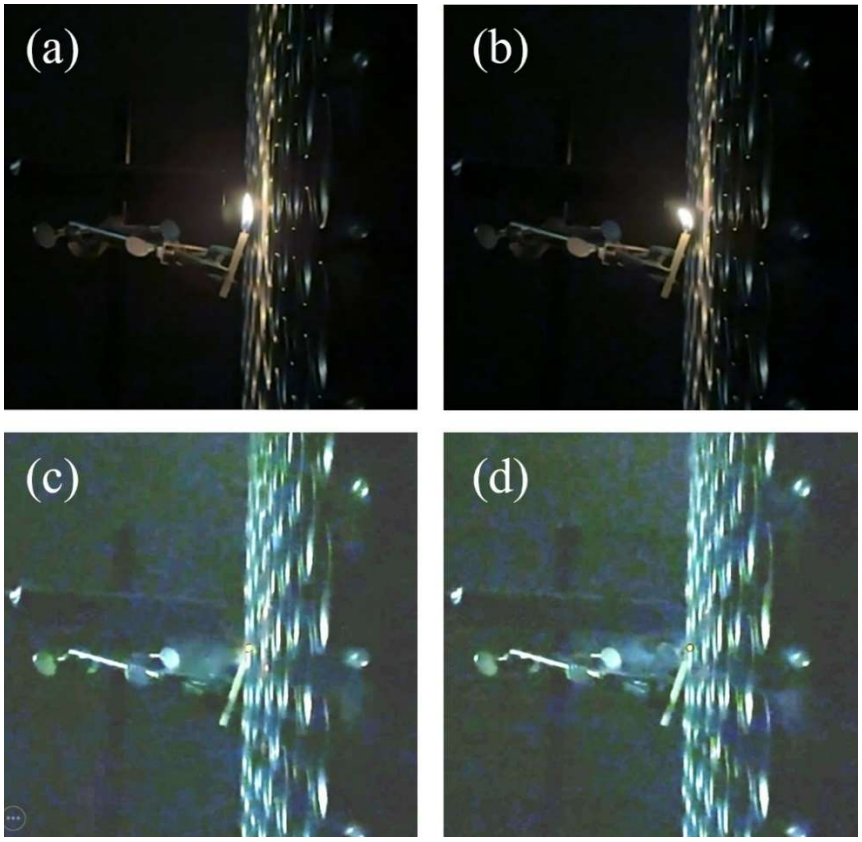

Figure 3.4 Photographs of a candle being blown out when TR focusing at sufficient amplitude near the resonator array. (a) candle lit. (b) flame is pushed outward. (c) and (d) show smoke trails blowing to the left, away from the array.

Testing for changes in the spatial extent of the TR focusing involved using the 2-D microphone scanning system. We first created a TR focus at the center can of the array and then proceeded to repeat the focusing while recording with the microphone at various locations along a vertical line scan of 161 locations starting from the top of the resonator array and ending at the bottom of the resonator array (passing through the focus location) with a spacing between points of 0.5 cm. Each time the microphone was moved, the same reversed impulse response signals were broadcast causing the same focusing to occur at the central can. We repeated the scan for a 100 mV input amplitude and a 1 V input. MATLAB (Natick, MA) was used to process the data and

plot the pressure amplitudes as a function of line scan position at the time of the maximum focusing.

A zero-padding method was used to essentially interpolate the data using the original spectral information. The results were zero-padded by making the spectrum possess 16 times the number of data points in the frequency spectrum, 1x being the data and 15x being zero values. The zero padded spectrum had the original spectral data below the Nyquist frequency as the lowest frequencies in the zero padded spectrum and then had the original spectral data above the Nyquist frequency (the mirrored part of the spectral amplitudes) as the highest frequencies in the zero padded spectrum with zeros in the middle. The inverse Fourier transform of this zero-padded spectrum yielded each zero-padded, spatial distribution of amplitudes plot. Figure 3.5(a) illustrates how the full width at half of the maximum (FWHM) value is determined by showing some plots of the spatial distribution of the focusing at the time of maximum amplitude. A squared 420 Hz wave (the highest frequency used in our bandwidth) is shown in blue to illustrate our definition of the diffraction limit, which uses the FWHM of the highest frequency in our bandwidth. The no-cans case yields a FWHM that is wider than the 420 Hz FWHM. The with-cans (low amplitude) plot yields a narrower FWHM than the diffraction limit result. Note that one of the dips between the main peak and the immediate side peak to the left does not dip below 0.5 but the right side does. The FWHM was calculated for four different cases with a ±0.5 cm uncertainty. The FWHM with no cans and low amplitude is 39.8 cm and at high amplitude is 39.4 cm (within the measurement uncertainty). The FWHM calculated with cans at low amplitude is 10.9 cm and at high amplitude is 14.6 cm. The FWHM for 420 Hz is 20.4 cm (the wavelength at 420 Hz is 81.7 cm). Figure 3.5(b) illustrates the scaled plots of the spatial distribution of the focusing at the time of maximum amplitude (the 100 mV result was multiplied by a factor of 10). The high amplitude

result is a lot lower in amplitude than linear scaling would predict it would be. At the respective maximum amplitudes, the peak is different by a factor of 3.08. Figure 3.5(c) illustrates normalized plots of the spatial distribution of the focusing at the time of maximum amplitude for both low and high amplitudes (each normalized with respect to their maximum values). The FWHM calculation is skewed at 0.5 with the asymmetry of the dips. Further, neither of the higher amplitude result's dips on either side of the largest peak dip below 0.5 so it skews the determination of FWHM even more. Thus the full width was measured at a couple of different normalized amplitudes, 0.25, 0.5, and 0.75. The 0.25 and 0.75 amplitudes offer more of a fair comparison since they have the same respective number of peaks inside them. The full width at a quarter of the maximum (FWQM) for the lower amplitude focusing is 16.8 cm while the high amplitude focusing resulted in 18.0 cm (a 7.1% increase). The FWHM with cans present and at low amplitude is 10.9 cm and at high amplitude is 14.6 cm (a 34% increase, though skewed). The full width at three fourths of the maximum (FWTQM) for the lower amplitude focusing is 3.7 cm while the high amplitude focusing resulted in 4.4 cm (a 20.4% increase).

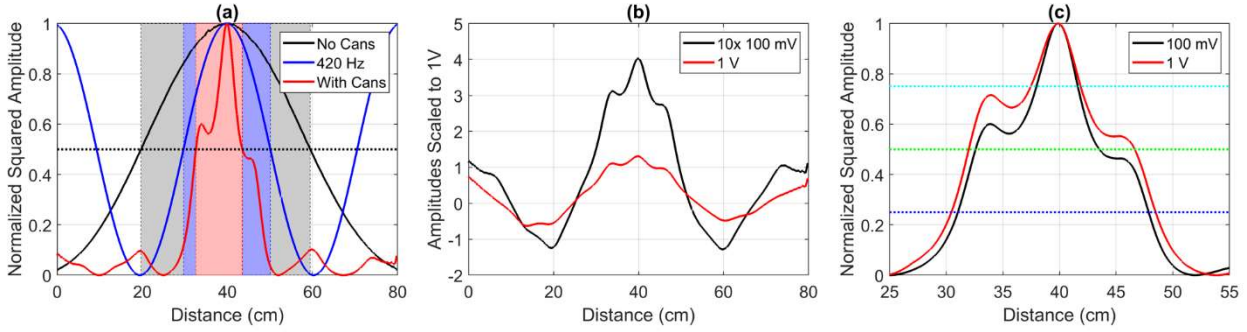

Figure 3.5 (a) Shows plots of the spatial distribution of focusing at the time of maximum amplitude along with a squared 420 Hz wave shown in blue to illustrate our diffraction limit definition. (b) Illustrates scaled plots of the spatial distribution of the focusing at the time of maximum amplitude for both low and high amplitudes. (c) Illustrates normalized plots of the spatial distribution of the focusing at the time of maximum amplitude for both low and high amplitudes. The full width is measured at 0.25, 0.5, and 0.75 normalized amplitudes, which values are indicated by the respective blue, green, and cyan dashed lines.

Chapter 4

Conclusion

Observations of nonlinear phenomena and their impact on TR focusing near an array of Helmholtz resonators has been investigated. TR focusing among an array of Helmholtz resonators is an effective method to produce sub-diffraction limited focusing, thereby increasing the spatial resolution of the focusing. It is important to be aware of the strong potential for nonlinear jetting that causes a nonlinear suppression of the amplitude of the focusing, a slight earlier arrival in time of that focusing, and a widening of the spatial extent of the focusing.

When simply increasing the input voltage amplitude and repeating TR focusing with the array present, the amplitude versus time graphs do not scale linearly, and instead a nonlinear suppression of both compressions and rarefactions is observed when comparing linearly scaled focusing results. The peak amplitude is reduced by about a factor of 3 relative to linear scaling when focusing at amplitudes of around 122.2 dB near a resonator array. Nonlinear suppression of focusing amplitudes is observed for essentially all input amplitudes used, even when comparing

input amplitude levels of 100 mV and 200 mV, though to a lesser extent. Our experiments were conducted between sound levels of 111.7 to 122.2 dB, so nonlinear phenomena at these levels was not initially expected. The peak amplitudes of the focusing also appear a little sooner in time than expected with increasing amplitude of focusing. These nonlinear phenomena are much less pronounced at sound levels of 111 dB and lower.

Helmholtz resonators appear to exhibit jetting, with these observations being more apparent at higher focusing amplitudes, which is likely the cause of the nonlinear phenomena altering the focus. When a candle is placed next to the resonator array, and sound is focused to the can adjacent to the candle, the flame visibly leans away from the cans over a period of tens of milliseconds (comprising about 10 periods of the central frequency used). These visual observations provide compelling evidence of jetting.

The spatial extent of the TR focusing when the resonator array is present is shown to be amplitude dependent. When the input amplitude is changed by a factor of 10, the focusing widens by about 20%. Since the amplitude of the focusing is nonlinearly suppressed as the input amplitude is increased, it makes sense that this would affect the highest amplitude in the TR focusing the most. A larger nonlinear reduction of the amplitude at the focal location would thus be expected than at the locations further away from the focal location that are not at as high of amplitudes, which would tend to widen the focusing.

Bibliography

[1] M. Fink, “Time reversed acoustics,” Phys. Today **50**(3), 34–40 (1997).

[2] B. E. Anderson, M. Griffa, C. Larmat, T. J. Ulrich, and P. A. Johnson, “Time reversal,” Acoust. Today **4**(1), 5-16 (2008).

[3] C. S. Clay and B. Anderson, “Matched signals: The beginnings of time reversal,” Proc. Meet. Acoust. **12**, 055001 (2011).

[4] B. E. Anderson, M. C. Remillieux, P.-Y. Le Bas, and T. J. Ulrich, “Time reversal techniques,” in Nonlinear Acoustic Techniques for Nondestructive Evaluation, 1st ed., edited by T. Kundu (Springer and Acoustical Society of America, New York, 2018), pp. 547–581.

[5] B. E. Anderson, “High amplitude time reversal focusing of sound and vibration,” Proc. Meet. Acoust. **51**, 032001 (2023).

[6] J.-L. Thomas, F. Wu, and M. Fink, “Time reversal focusing applied to lithotripsy,” Ultrason. Imag. **18**(2), 106–121 (1996).

[7] M. Tanter, J.-L. Thomas, and M. Fink, “Focusing and steering through absorbing and aberrating layers: Application to ultrasonic propagation through the skull,” J. Acoust. Soc. Am. **103**(5), 2403–2410 (1998).

[8] G. Montaldo, P. Roux, A. Derode, C. Negreira, and M. Fink, “Ultrasound shock wave generator with one-bit time reversal in a dispersive medium, application to lithotripsy,” Appl. Phys. Lett. **80**, 897–899 (2002).

[9] B. E. Anderson, M. Griffa, T. J. Ulrich, P.-Y. Le Bas, R. A. Guyer, and P. A. Johnson, "Crack localization and characterization in solid media using time reversal techniques," Am. Rock Mech. Assoc., #10-154 (2010).

[10] C. Heaton, B. E. Anderson, and S. M. Young, "Time reversal focusing of elastic waves in plates for educational demonstration purposes," J. Acoust. Soc. Am. **141**(2), 1084-1092 (2017).

[11] L. A. Barnes, B. E. Anderson, P.-Y. Le Bas, A. D. Kingsley, A. C. Brown, and H. R. Thomsen, "The physics of knocking over LEGO minifigures with time reversal focused vibrations," J. Acoust. Soc. Am. **151**(2), 738-751 (2022).

[12] J. M. Cliftmann and B. E. Anderson, "Remotely extinguishing flames through transient acoustic streaming using time reversal focusing of sound," Sci. Rep. **14**, 30049 (2024).

[13] D. G. Albert, L. Liu, and M. L. Moran, "Time reversal processing for source location in an urban environment (L)," J. Acoust. Soc. Am. **118**(2), 616–619 (2005).

[14] S. Cheinet, L. Ehrhardt, and T. Broglin, "Impulse source localization in an urban environment: time reversal versus time matching," J. Acoust. Soc. Am. **139**(1), 128–140 (2016).

[15] C. Larmat, J.-P. Montagner, M. Fink, Y. Capdeville, A. Tourin, and E. Clevede, "Time reversal imaging of seismic sources and applications to the great Sumatra earthquake," Geophys. Res. Lett. **33**(19), L19312 (2006).

[16] C. Larmat, J. Tromp, Q. Liu, and J.-P. Montagner, "Time-reversal location of glacial earthquakes," J. Geophys. Res. **113**(B9), B09314 (2008).

[17] C. Larmat, R. A. Guyer, and P. A. Johnson, "Tremor source location using time-reversal: selecting the appropriate imaging field," Geophys. Res. Lett. **36**(22), L22304 (2009).

[18] C. S. Larmat, R. A. Guyer, and P. A. Johnson, "Time-reversal methods in geophysics," Phys. Today **63**(8), 31–35 (2010).

[19] T. S. Furlong, B. E. Anderson, B. D. Patchett, and S. D. Sommerfeldt, "Active noise control using remotely placed sources: Application to magnetic resonance imaging noise and equivalence to the time reversal inverse filter," Appl. Acoust. **176**, 107902 (2021).

[20] H. C. Song, "An overview of underwater time-reversal communication," IEEE J. Oceanic Eng. **41**, 644–655 (2016).

[21] B. E. Anderson, T. J. Ulrich, P.-Y. Le Bas, and J. A. Ten Cate, "Three dimensional time reversal communications in elastic media," J. Acoust. Soc. Am. **139**(2), EL25-EL30 (2016).

[22] H. C. Song and W. A. Kuperman, "Time machine in ocean acoustics," J. Acoust. Soc. Am. **153**(1), R1–R2 (2023).

[23] G. Lerosey, J. de Rosny, A. Tourin, and M. Fink, "Focusing beyond the diffraction limit with far-field time reversal," Science **315**(5815), 1120–1122 (2007).

[24] F. Lemoult, M. Fink, and G. Lerosey, "Acoustic Resonators for Far-Field Control of Sound on a Subwavelength Scale," Phys. Rev. Lett. **107,** 064301 (2011).

[25] F. Lemoult, N. Kaina, M. Fink, and G. Lerosey, "Wave propagation control at the deep subwavelength scale in metamaterials," Nat. Phys. **9**, 55-60 (2013).

[26] A. A. Maznev, G. Gu, S.-Y. Sun, J. Xu, Y. Shen, N. Fang, and S.-Y. Zhang, "Extraordinary focusing of sound above a soda can array without time reversal," New J. Phys. **17**, 042001 (2015).

[27] F. Lemoult, N. Kaina, M. Fink, and G. Lerosey, "Soda cans metamaterial: A subwavelength scaled phononic crystal," Crystals, **6**(7) 82 (2016).

[28] A. A. Maznev and O. B. Wright, "Upholding the diffraction limit in the focusing of light and sound," Wave Motion **68**, 182-189 (2017).

[29] B. Orazbayev and R. Fleury, "Far-field subwavelength acoustic imaging by deep learning," Phys. Rev. X **10**, 031029 (2020).

[30] A. D. Kingsley, B. E. Anderson, and T. J. Ulrich, "Super-resolution within a one-dimensional phononic crystal of resonators using time reversal in an equivalent circuit model," J. Acoust. Soc. Am. **152**(3), 1263-1271 (2022).

[31] A. D. Kingsley and B. E. Anderson, "Time reversal in a phononic crystal using finite-element modeling and an equivalent circuit model," JASA Exp. Lett. **2**(12), 124002 (2022).

[32] A. D. Kingsley, A. Basham, and B. E. Anderson, "Time reversal imaging of complex sources in a 3-dimensional environment using a spatial inverse filter," J. Acoust. Soc. Am. **154**(2), 1018-1027 (2023).

[33] A. Basham, B. E. Anderson, and A. D. Kingsley, "Improving super resolution in time reversal focusing among a resonator array metamaterial by restricting the angle of incidence," J. Acoust. Soc. Am. **155**(5), 3233-3241 (2024).

[34] G. Montaldo, P. Roux, A. Derode, C. Negreira, and M. Fink, "Ultrasound shock wave generator with one-bit time reversal in a dispersive medium, application to lithotripsy," Appl. Phys. Lett. **80**(5), 897–899 (2002).

[35] M. L. Willardson, B. E. Anderson, S. M. Young, M. H. Denison, and B. D. Patchett, "Time reversal focusing of high amplitude sound in a reverberation chamber," J. Acoust. Soc. Am. **143,** 696–705 (2018).

[36] B. D. Patchett and B. E. Anderson, "Nonlinear characteristics of high amplitude focusing using time reversal in a reverberation chamber," J. Acoust. Soc. Am. **151**(6), 3603-3614 (2022).

[37] B. D. Patchett, B. E. Anderson, and A. D. Kingsley, "Numerical modeling of Mach-stem formation in high-amplitude time-reversal focusing," J. Acoust. Soc. Am. **153**(5), 2724-2732 (2023).

[38] C. B. Wallace and B. E. Anderson, "High-amplitude time reversal focusing of airborne ultrasound to generate a focused nonlinear difference frequency," J. Acoust. Soc. Am. **150**(2), 1411-1423 (2021).

[39] D. Russell, "Acoustic Rocket Demonstration – revisiting Dvorak's 1878 Acoustic Repulsion Apparatus," https://youtu.be/TQ1_B1Wo03s (Last viewed June 20, 2025).

[40] B. E. Anderson, M. Clemens, and M. L. Willardson, "The effect of transducer directionality on time reversal focusing," J. Acoust. Soc. Am. **142**(1), EL95–EL101 (2017).

[41] B. Van Damme, K. Van Den Abeele, Y. Li, and O. Bou Matar, “Time reversed acoustics techniques for elastic imaging in reverberant and nonreverberant media: An experimental study of the chaotic cavity transducer concept,” J. Appl. Phys. **109**(10), 104910 (2011).

[42] A. D. Kingsley, J. M. Clift, B. E. Anderson, J. E. Ellsworth, T. J. Ulrich, and P.-Y. Le Bas, “Development of software for performing acoustic time reversal with multiple inputs and outputs,” Proc. Meet. Acoust. **46**, 055003 (2022).